JOURNAL OF MATERIALS SCIENCE 21 (1986) 4269–4280

The effect of isothermal exposure on the transverse properties of a continuous fibre metal-matrix composite

TETSUYUKI KYONO*, IAN W. HALL
Department of Mechanical and Aerospace Engineering, University of Delaware, Newark, Delaware 19716, USA

MINORU TAYA
Department of Mechanical Engineering, FU-10, University of Washington, Seattle, Washington 98195, USA

The effect of isothermal exposure at 500° C on the transverse mechanical properties of 30 and 50 vol% continuous boron-fibre reinforced 1100 aluminium composites has been investigated. Experimental results indicate that the fibre–matrix interfacial reaction gives rise to an increase in the fibre–matrix bond strength. Consequently, the fracture mode undergoes a transition from interfacial debonding to fibre splitting with increasing exposure time. The fracture surfaces and fibre–matrix interfaces have been studied by scanning electron microscopy and the observations coincide with the above interpretation of the mechanical test results. Finally, a new theoretical model using Eshelby's theory is developed to analyse the stress–strain behaviour of a continuous fibre reinforced metal matrix composite subjected to transverse tensile loading.

1. Introduction

Continuous fibre reinforced metal matrix composites (MMCs) are generally considered to be attractive as structural engineering materials because of their superiority to polymer–matrix composites for high temperature use as well as their outstanding specific stiffness and strength. Since these attractive properties are displayed in the longitudinal direction of the reinforcing fibre, emphasis has been placed on the enhancement of the longitudinal stiffness (E_L), strength (σ_{UL}) and toughness (γ_F) [1]. Thus, it has been known that σ_{UL} and γ_F in particular are strongly affected not only by the fibre volume fraction but also by the structure of the fibre–matrix interface, which is itself affected by the thermal history of the MMC during fabrication and/or subsequent service. That is, too strong a fibre–matrix bond coupled with a reduction of the fibre strength due to the fibre–matrix reaction is found to cause remarkable reductions in σ_{UL} and γ_F [1–3].

On the other hand, higher values of the transverse strength (σ_{UT}), which are considered to depend on the fibre–matrix bond strength as well as the mechanical properties of the matrix itself [1], are very desirable for some applications. Unfortunately, the requirements for σ_{UL} and γ_F of a continuous fibre MMC often conflict with those for σ_{UT}. Therefore, a study on the transverse properties of the composite is equally important from the design point of view. Several studies have been made concerning the transverse properties of MMCs [3–10]. For example, Adams and co-workers [4, 5] analysed both elastic and inelastic transverse tensile behaviour of a MMC microscopically by the finite element method, and Lin *et al.* [6] related the σ_{UT} to the fibre volume fraction for MMCs with two different fibre–matrix bond strengths. However, no attempt has been made to correlate the transverse tensile properties and stress–strain behaviour to the fibre–matrix interfacial reaction at elevated temperature except for the work of Amateau and Dull [7].

In this paper we will report on the room-temperature values of σ_{UL} and σ_{UT} of a continuous fibre reinforced MMC subjected to isothermal high temperature exposure. Based on the present experimental results, we attempt to analyse the transverse tensile stress–strain behaviour of the composite using Eshelby's theory [11].

2. Experimental procedure

2.1. Materials

Unidirectional boron fibre reinforced aluminium composites (B–Al composites) were obtained as sheet panels from AVCO Specialty Materials Division (Lowell, Massachusetts). The 8-ply panels were diffusion-bonded using a proprietary technique. The boron fibre used in this study is 102 μm in diameter and the volume fractions of the composites are 0.3 and 0.5. 1100 aluminium was selected as the matrix alloy in order to avoid as far as possible the presence of any second phase or precipitate particles in the matrix,

*On leave from Pioneering R & D Laboratories, Toray Industries, Inc., 2-1, 3-chome, Sonoyama, Otsu, Shiga 520, Japan.

0022–2461/86 $03.00 + .12

such as occur in typical aluminium alloys and which might affect σ_{UL} and σ_{UT}, particularly σ_{UT}, after the isothermal exposure. The mechanical properties of both constituents are $\sigma_{fu} = 3.52\,GPa$, $E_f = 400\,GPa$ and $v_f = 0.21$ [12] for boron fibre and $\sigma_{mu} = 89.6\,MPa$, $E_m = 69\,GPa$, $\sigma_y = 35\,MPa$ and $v_m = 0.33$ for 1100 aluminium, where σ_{iu}, E_i and v_i are ultimate tensile strength, Young's modulus and Poisson's ratio of the i phase (i = f or m), respectively, and σ_y is tensile yield stress of the matrix.

2.2. Isothermal exposure

B–Al test coupons were exposed to 500° C in argon for times (t) of 1, 8, 24 or 72 h. Although 500° C is considerably higher than any conceivable temperature which might be met in service, this temperature was chosen as it is known to be sufficient to cause marked changes in the longitudinal tensile properties of the composite and should allow rapid formation of fibre–matrix interfacial reaction products [2, 13].

2.3. Tensile tests of composites

Both longitudinal and transverse tensile tests were carried out on as-fabricated as well as isothermally exposed composites. Specimens for longitudinal tests were 152.4 mm long, 12.7 mm wide and 1.27 mm thick for $V_f = 0.3$ and 0.88 mm thick for $V_f = 0.5$, respectively, and those for transverse tensile tests differed only by being 25.4 mm wide. Strain gauges were mounted to the middle of the gauge length (76.2 mm), and aluminium end-tabs were adhesively bonded to each side of the specimen in the grip area. All tests were conducted at room temperature by using a standard Instron machine at a strain rate of $6.7 \times 10^{-3}\,min^{-1}$.

2.4. Scanning electron microscopy

The fracture surfaces of the B–Al composite after the tensile tests, and the surface morphology of fibres extracted from both the as-fabricated and isothermally exposed composites, were observed using a Philips 501 scanning electron microscope (SEM).

2.5. Hardness measurements

In order to investigate the effect of isothermal exposure on the yield stress and tensile strength of the matrix itself, microhardness tests were carried out using a Vickers microhardness tester and a load of 10 g. Care was taken to ensure that the position of the hardness impression was as far as possible from the fibres or the reaction zone. Five hardness measurements were taken for each exposure time and statistical data such as the mean value, standard deviation and coefficient of variation were obtained.

3. Results and discussion

The longitudinal (σ_{UL}) and transverse (σ_{UT}) tensile strengths are plotted as a function of exposure time (t) in Figs 1 and 2, respectively, where open symbols and vertical lines denote the mean values and band of scattered data, respectively. It can be seen from Figs 1 and 2 that σ_{UL} decreases beyond $t \simeq 8$ h, while σ_{UT} increases gradually with t. In order to aid in explaining the above observation, the fracture surfaces of both longitudinally and transversely tested coupons were examined by SEM and typical fractographs and shown in Figs 3 and 4. As the exposure time is increased, the fracture surfaces of longitudinally tested coupons tend to become flatter with less fibre pull-out, while in transversely tested coupons fibre splitting becomes dominant. These observations reveal that the fibre–matrix bond strength increased due to the chemical reaction between the two constituents with increasing exposure time.

Based on the analytical work of Mikata and Taya [14], circumferential cracks can form in the brittle reaction layer of longitudinally tested coupons due to the high tensile stress along the fibre axis, resulting in a loss of the longitudinal strength. In the case of transversely tested coupons, the high circumferential stress in the reaction layer can cause a splitting type crack. Once the splitting type crack has occurred in the reaction layer during transverse tensile loading, it can propagate further into the fibre, thus causing fibre splitting or interfacial debonding. The surfaces of

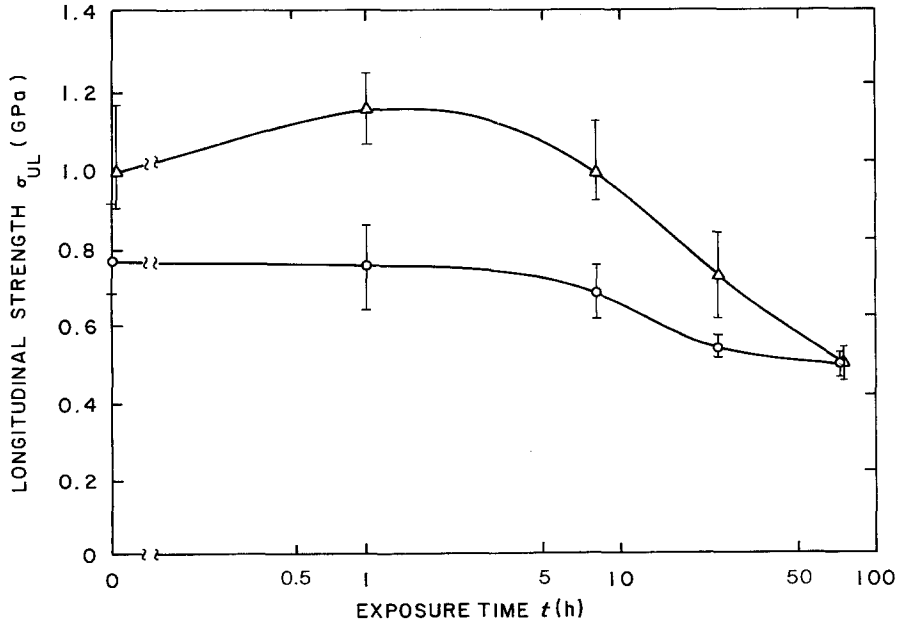

Figure 1 Longitudinal strength (σ_{UL}) of thermally exposed B–Al as a function of exposure time (t) at 500° C. (○) $V_f = 0.3$, (△) $V_f = 0.5$.

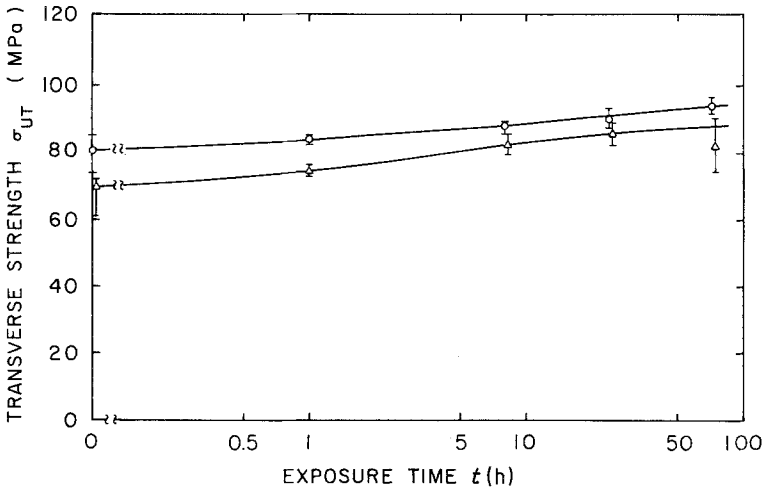

Figure 2 Transverse strength (σ_{UT}) of thermally exposed B–Al as a function of exposure time (t) at 500° C. (○) $V_f = 0.3$, (△) $V_f = 0.5$.

fibres extracted from as-fabricated and thermally exposed composites are shown in Fig. 5. The latter surface was covered with small angular crystals which were identified by X-ray diffraction techniques mainly as AlB_2 [1, 2, 15].

The transverse tensile stress–strain curves of B–Al composites are plotted as a function of exposure time in Fig. 6, where the symbols denote the fracture points of composites subjected to different exposure times. It is to be noted that the stress–strain curves exhibit two stages, linear and non-linear, and the curve is more likely to rise as the exposure time is increased, except for the as-fabricated case.

The results of microhardness testing of the matrix are plotted in Fig. 7, where open symbols and vertical lines denote the mean values and band of scattered data, respectively. It can be seen from Fig. 7 that the microhardness, which is related to the flow stress of the matrix, decreases for the shorter exposure time and then increases slightly for longer exposure time. The reason that the flow stress of the as-fabricated matrix metal is relatively high is due to the work hardening during the fabrication process [16].

The above dependence of the matrix flow stress on the exposure time t can explain partially the trend of the stress–strain curves in Fig. 6. It is also noted from Fig. 6 that the fracture strain, ε_f, of $V_f = 0.5$ composite is much smaller than that of $V_f = 0.3$ composite. This can be explained as follows. In the $V_f = 0.5$ composite, the volume fraction of brittle phases (fibres with or without a reaction zone) is larger and mini-cracks are more likely to be formed in the brittle phases at higher applied stress. Once these cracks are formed, they can propagate easily with increasing applied stress, resulting in the coalescence of these mini-cracks, and followed by the final fracture of the composite. The volume fraction of the ductile phase (matrix metal), which would serve as a crack arrester, is smaller in the $V_f = 0.5$ composite and, hence, the fracture strain is lower.

4. Analytical studies

An attempt is made to construct analytical models to explain the trend of the transverse stress–strain curves of B–Al composites.

The transverse tensile stress–strain curves of B–Al composites show two stages, linear and non-linear as described in the previous section. In the linear stage,

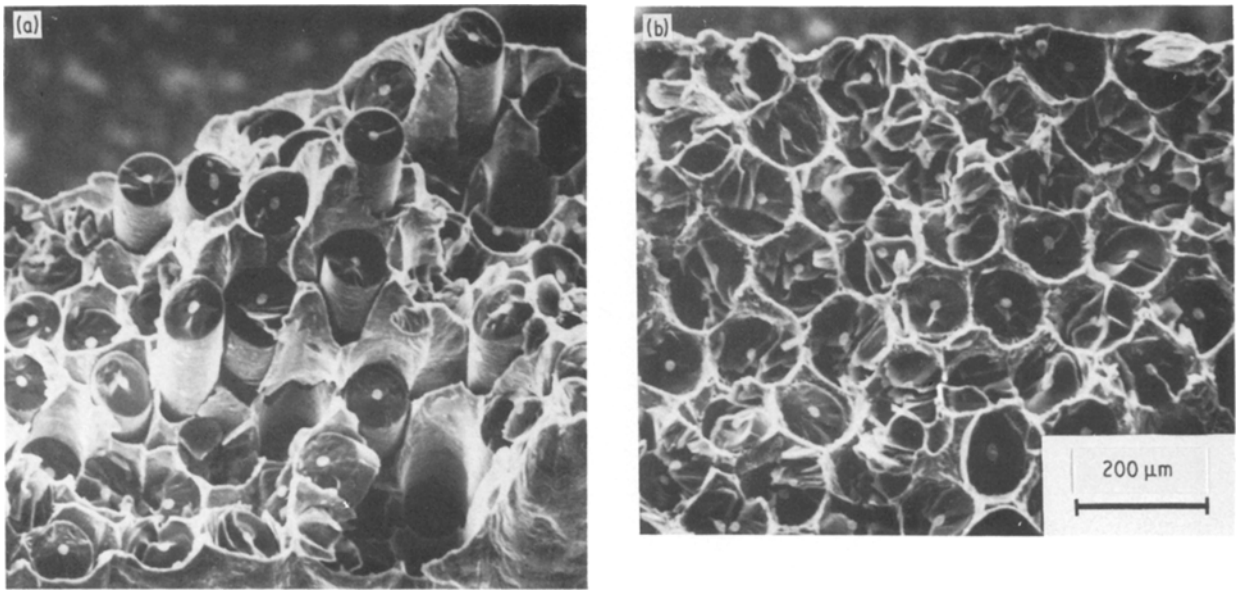

Figure 3 SEM photographs of the fracture surfaces of the longitudinally tensile tested B–Al for (a) as-fabricated and (b) exposed at 500° C for 72 h.

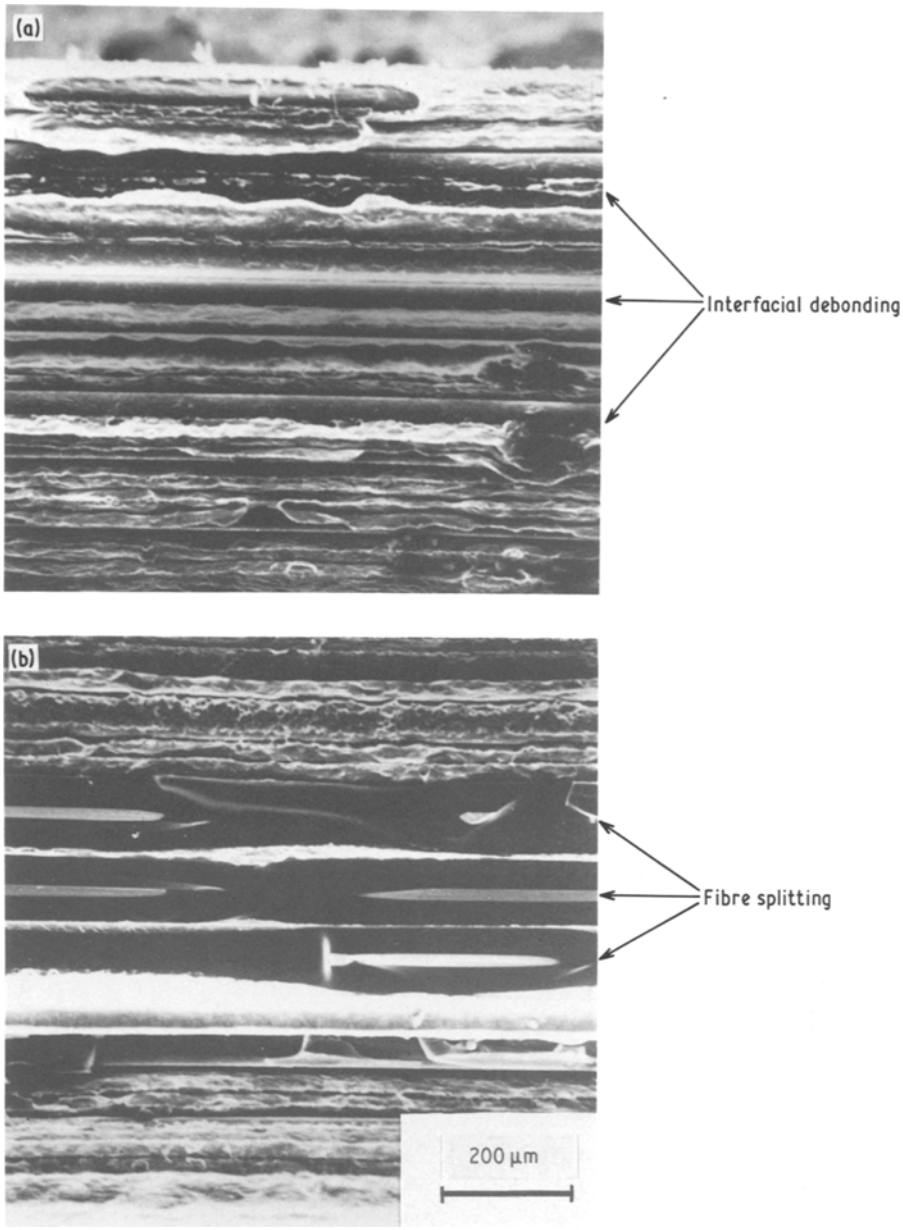

Figure 4 SEM photographs of the fracture surfaces of the transversely tensile tested B–Al for (a) as-fabricated and (b) exposed at 500° C for 72 h.

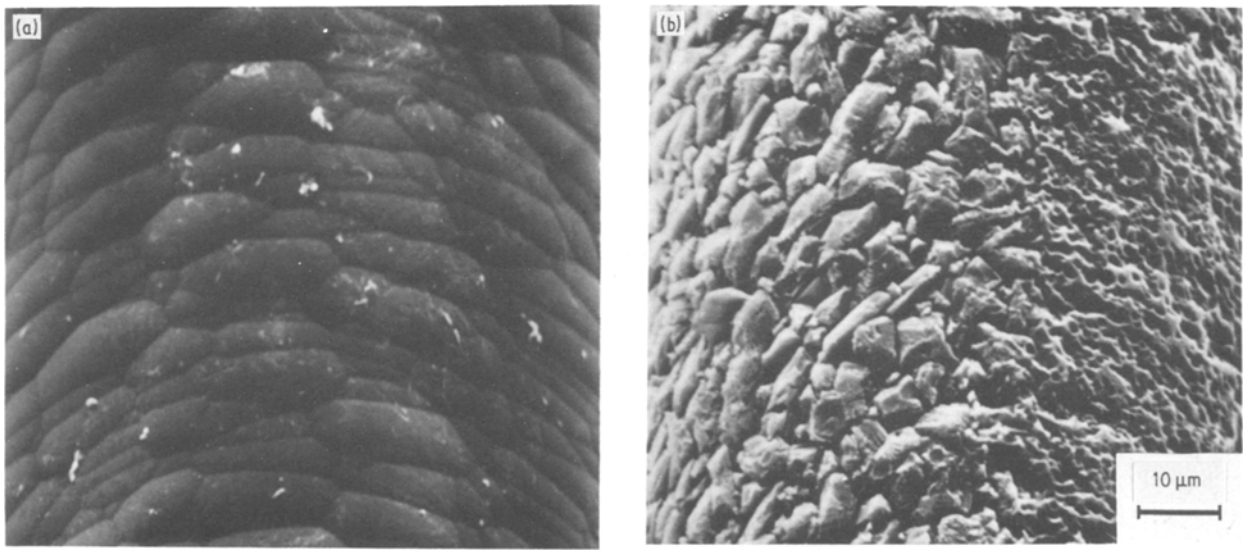

Figure 5 SEM photographs of the surfaces of boron fibres extracted from the composites for (a) as-fabricated and (b) exposed at 500° C for 72 h.

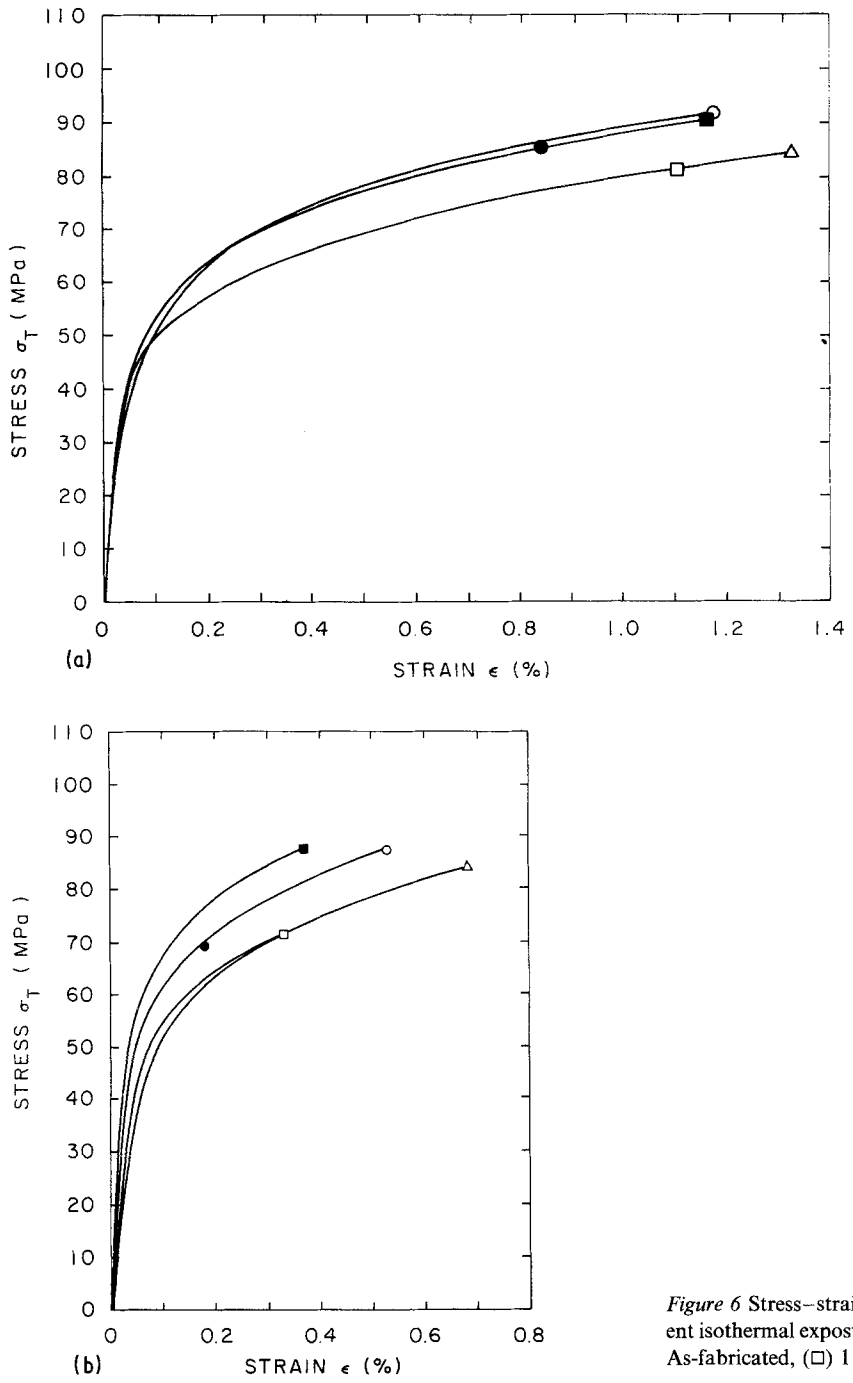

Figure 6 Stress–strain curves obtained experimentally after different isothermal exposure times for (a) $V_f = 0.3$ and (b) $V_f = 0.5$. (●) As-fabricated, (□) 1 h, (△) 8 h, (○) 24 h, (■) 72 h.

the fibre–matrix interface is considered to be perfectly bonded and both matrix and fibre deform elastically under the applied stress σ_{ij}^0. However, the slopes of the linear stage for B–Al composites exposed for different times do not coincide except for the initial part of the linear stage. Thus, it is believed that in the thermally exposed composite, some fibres were not well bonded to the matrix even in the linear stage of the stress–strain curve. In the non-linear stage, several possible micromechanical modes of deformation can be considered, for example, plastic deformation in the matrix and the debonding of the fibre–matrix interface.

Based on the above discussion, we have constructed two models to simulate the behaviour of the transverse tensile stress–strain curve. Figs 8 and 9 are the analytical models for the linear stage and non-linear stage, respectively, where the fibre axis is taken along the X_3 axis. In the linear stage model, both the matrix and fibres (shaded in Fig. 8) are assumed to deform elastically, while it is assumed in the non-linear stage model (Fig. 9) that the fibres deform elastically but the matrix deforms plastically with uniform plastic strain $(\varepsilon, -\varepsilon/2, -\varepsilon/2)$ [17, 18]. In both models Eshelby's equivalent inclusion method will be applied. A detailed description of these two models will be given below.

4.1. Linear stage model

In this model (see Fig. 8), two different types of inhomogeneities are embedded in an infinite matrix, i.e., perfectly bonded fibres (Ω_A) and debonded fibres (Ω_B). Thus, the system of Fig. 8 can be considered as a hybrid composite. Let the elastic constants of the matrix and fibre Ω_A and Ω_B be C_{ijkl}^0 and C_{ijkl}, respectively. The volume fractions of Ω_A and Ω_B are denoted by f_A and f_B, respectively.

Under the applied stress σ_{ij}^0, the average total stress in the matrix is given by $\sigma_{ij}^0 + \langle \sigma_{ij} \rangle_M$ [17–21] and

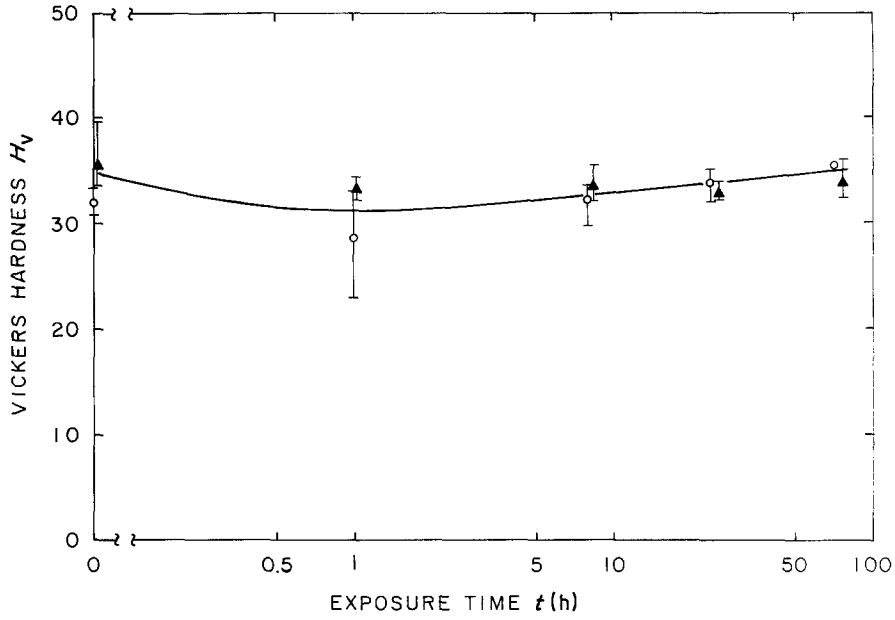

Figure 7 Vickers microhardness of the matrix (H_v^{10}) as a function of exposure time (t). (○) $V_f = 0.3$, (▲) $V_f = 0.5$.

$$\langle \sigma_{ij} \rangle_M = C^0_{ijkl} \tilde{e}_{kl} \quad (1)$$

where $\langle \sigma_{ij} \rangle_M$ and $\tilde{e}_{kl}$ are the average stress and strain disturbances of the matrix due to all Ω_A and Ω_B, respectively, and $\langle\ \rangle$ denotes the volume averaged quantity. The repeated subscripts are to be summed over 1, 2 and 3 (this convention will be used throughout this paper unless otherwise noted). If a single fibre is introduced into the composite (D), then Eshelby's equivalent inclusion method [17–21] yields in D

$$\begin{aligned} \sigma^0_{ij} + \sigma^i_{ij} &= C_{ijkl}(e^0_{kl} + \tilde{e}_{kl} + e^i_{kl}) \\ &= C^0_{ijkl}(e^0_{kl} + \tilde{e}_{kl} + e^i_{kl} - e^{i*}_{kl}) \end{aligned} \quad (2)$$

where σ^i_{ij} and e^i_{ij} are the disturbance of the stress and strain due to a single Ω_i, respectively, with the superscript i being A or B. e^{i*}_{kl} is the corresponding eigenstrain which has non-vanishing components in the domain of this single Ω_i and becomes zero outside Ω_i. For the entire composite domain D the following relation always holds:

$$\sigma^0_{ij} = C^0_{ijkl} e^0_{kl} \quad (3)$$

With Equation 3, Equation 2 yields

$$\sigma^i_{ij} = C^0_{ijkl}(\tilde{e}_{kl} + e^i_{kl} - e^{i*}_{kl}) \quad (4)$$

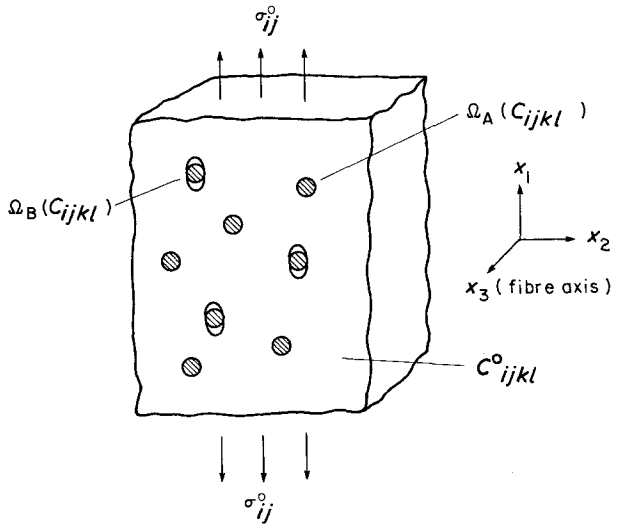

Figure 8 Analytical model for the linear stage.

Following Eshelby [11], we have

$$e^i_{kl} = S_{klmn} e^{i*}_{mn} \quad \text{in } \Omega_i \quad (5)$$

where S_{klmn} is Eshelby's tensor which depends on C^0_{ijkl} and the geometry of Ω_i. In our case Ω_A and Ω_B have the same S_{klmn}.

By assuming that the second inhomogeneities (Ω_B) are debonded fibres, we obtain [22]

$$\sigma^0_{11} + \sigma^B_{11} = 0 \quad (6)$$

Except for Equation 6, all the equations up to Equation 5 are also valid for Ω_B. Since the integral of the stress disturbance over the entire domain D vanishes [20], we obtain

$$(1 - f_A - f_B)\langle \sigma_{ij} \rangle_M + f_A \langle \sigma^A_{ij} \rangle_{\Omega_A} + f_B \langle \sigma^B_{ij} \rangle_{\Omega_B} = 0 \quad (7)$$

Three unknowns $\tilde{e}_{ij}$, e^{A*}_{ij}, e^{B*}_{ij} will be solved by using Equations 2 to 7. Once e^{A*}_{ij} and e^{B*}_{ij} are solved, we can compute the initial overall stiffness of the composite by using the equivalence of the strain energies [20, 21] given by

$$\begin{aligned} \tfrac{1}{2}\sigma^0_{ij}(C^c_{ijkl})^{-1}\sigma^0_{kl} &= \tfrac{1}{2}\sigma^0_{ij}(C^0_{ijkl})^{-1}\sigma^\circ_{kl} + \tfrac{1}{2} f_A \sigma^0_{ij} e^{A*}_{kl} \\ &\quad + \tfrac{1}{2} f_B \sigma^0_{ij} e^{B*}_{kl} \end{aligned} \quad (8)$$

where $(C^0_{ijkl})^{-1}$ and $(C^c_{ijkl})^{-1}$ are the compliances of the matrix and composite, respectively. The details of the derivation of equation 8 are described by Taya and Chou [20].

We consider here the uniaxially applied stress σ^0 along the x_1 axis as shown in Fig. 8. Then the initial transverse Young's modulus E_T of the composite can be obtained as

$$\frac{E_T}{E_m} = \left[1 + \frac{E_m}{\sigma^0}(f_A e^{A*}_{11} + f_B e^{B*}_{11})\right]^{-1} \quad (9)$$

where E_m is the Young's modulus of the matrix and e^{A*}_{11}, e^{B*}_{11} are eigenstrains given by

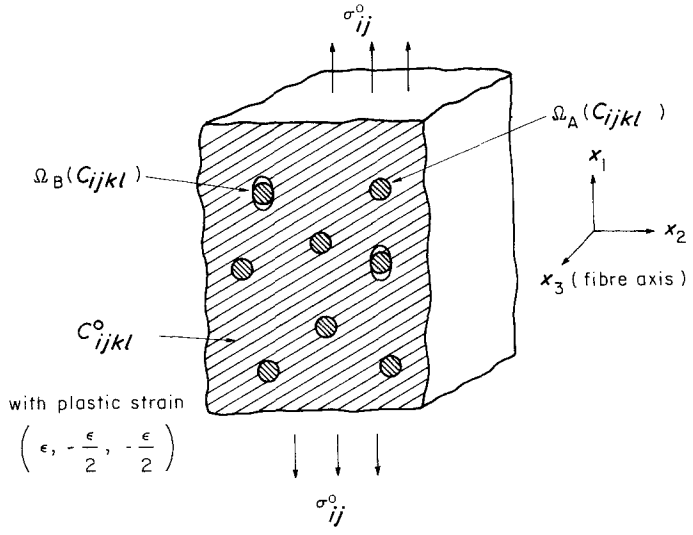

Figure 9 Analytical model for the non-linear stage.

$$e_{11}^{A*} = F_{11}^{A}\left(\frac{\sigma_0}{E_m}\right)$$
$$e_{11}^{B*} = F_{11}^{B*}\left(\frac{\sigma_0}{E_m}\right) \quad (10)$$

F_{11}^{A} and F_{11}^{B} are given in Appendix A. Thus, the key parameters of Equation 9 are the volume fractions of Ω_A (f_A) and Ω_B (f_B). Note that $f_A + f_B = V_f$, where V_f is the volume fraction of the fibres (both perfectly bonded and debonded fibres).

4.2. Non-linear stage model

As regards the non-linear stage model (see Fig. 9), most of the formulae used for the linear stage model are also applicable to this model. As far as the computation of the total potential energy and the internal stress field in the composite are concerned, the model of Fig. 9 is equivalent to a model in which the plastic strain with opposite sign is prescribed in the fibres and the matrix remains elastic under the applied stress σ^0_{ij} [17, 18]. Following the model developed in earlier work [17, 18] we obtained the relationship between the transversely applied stress (σ_T) and plastic strain (ε) for the non-linear stage which is linearized as

$$\sigma_T = K_1\sigma_y + K_2 E\varepsilon \quad (11)$$

where K_1 and K_2 are functions of f_A and f_B as described in Appendices A and B, and σ_y is the yield stress of the matrix which is assumed to be constant. Thus, the key parameters of Equation 11 are K_1 and K_2, i.e. the volume fraction of f_B. It should be noted here that the above model (Equation 11) is valid only for the early part of the non-linear stage [23], hence it is not applicable for the prediction of the fracture point of the stress–strain curve.

4.3. Estimation of f_B

In order to apply the analytical results of Equation 11 to predict the early part of the non-linear stage of the stress–strain curve, one must develop a micromechanical model which can relate the stress during transverse loading (σ_T) to the bond strength of the matrix–fibre interface (σ_i) as well as a relationship between f_B and σ_i. Before constructing such a relationship, we have first conducted a parametric study to obtain a series of bi-linear stress–strain curves defined by Equations 9 and 11 for given values of f_B. The results are shown in Fig. 10 for the case of $t = 24$ h and $V_f = 0.5$. In the same figure the corresponding experimental results are plotted as a thick solid curve. Since the volume fraction of debonded fibres (f_B) is expected to increase with an increase in the applied stress (σ_T), the actual path of the non-linear stage of the stress–strain curve is to undergo a continuous shift from $f_B = 0$ to increasing values of f_B, thus following the experimental curve (thick solid curve) in principle. To make the present model complete, we now assume that the bond strength (σ_i) follows a three-parameter Weibull distribution given by

$$f(\sigma_i) = \frac{m(\sigma_i - \gamma)^{m-1}}{\alpha}\exp\left(-\frac{(\sigma_i - \gamma)^m}{\alpha}\right) \quad (\sigma_i \geqq \gamma)$$
$$= 0 \quad (\sigma_i < \gamma) \quad (12)$$

$$F(\sigma_i) = 1 - \exp\left(-\frac{(\sigma_i - \gamma)^m}{\alpha}\right) \quad (\sigma_i \geqq \gamma) \quad (13)$$

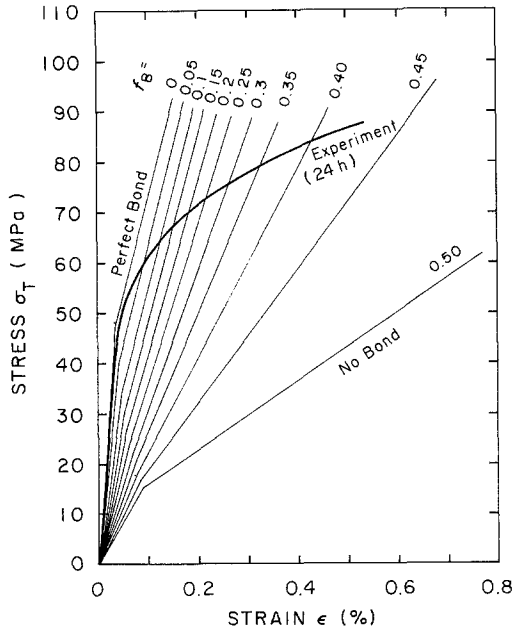

Figure 10 Schematic diagram to correlate the volume fraction of the debonded fibre (f_B) with the interfacial stress (σ_i) at Point A in Fig. 11, for B–Al with $V_f = 0.5$.

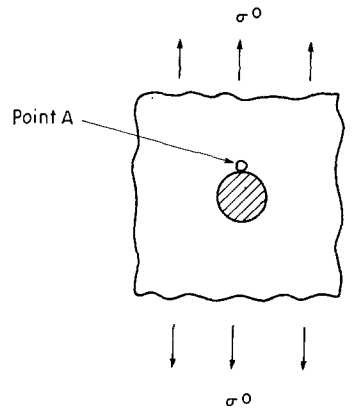

Figure 11 The normal stress along the loading direction at Point A is set equal to the bond strength of the fibre–matrix interface for the criterion of the debonding of the interface.

where $f(\sigma_i)$ and $F(\sigma_i)$ are the probability density function and cumulative distribution function of fibre–matrix bond strength (σ_i), respectively, and m, α and γ are called the shape parameter, scale parameter and location parameter, respectively. Based on the assumption that f_B increases continuously as the applied stress is increased up to the failure of the composite, f_B is set equal to $F(\sigma_i)$ in Equation 13. Thus, we have computed the fibre–matrix interfacial stress causing the debonding at point A (see Fig. 11), which is equal to the fibre–matrix bond strength during transverse tensile loading with different exposure conditions; the results are plotted in Fig. 12, where Figs 12a and b denote the cases of $V_f = 0.3$ and 0.5, respectively. We can now estimate the values of m and α from Fig. 12 and Equation 13, and they are found as $m = 1.05$, $\alpha = 91.69$.

4.4. Prediction of stress–strain curves

Based on the discussion in previous sections, an attempt is made to obtain theoretical stress–strain curves. To this end, the value of γ (which cannot be determined from Fig. 12) must be known. γ is considered to be the initial value at which the debonding begins to occur in the transversely tensile tested composite, and plays an important role in Fig. 12. Three case studies made are as follows:

(i) $\gamma = 44.8$ MPa ($= 0.5\sigma_{mu}$, weak interface);
(ii) $\gamma = 70.0$ MPa (intermediate interface);
(iii) $\gamma = 89.6$ MPa ($= \sigma_{mu}$, strong interface).

The probability density function of the bond strength, $f(\sigma_i)$, and Equation 12 for the above value of γ are shown in Fig. 13, where the values of the bond strength beyond 260 MPa are not adopted for the present analysis because the fracture mode of the transversely tested composite is supposed to change

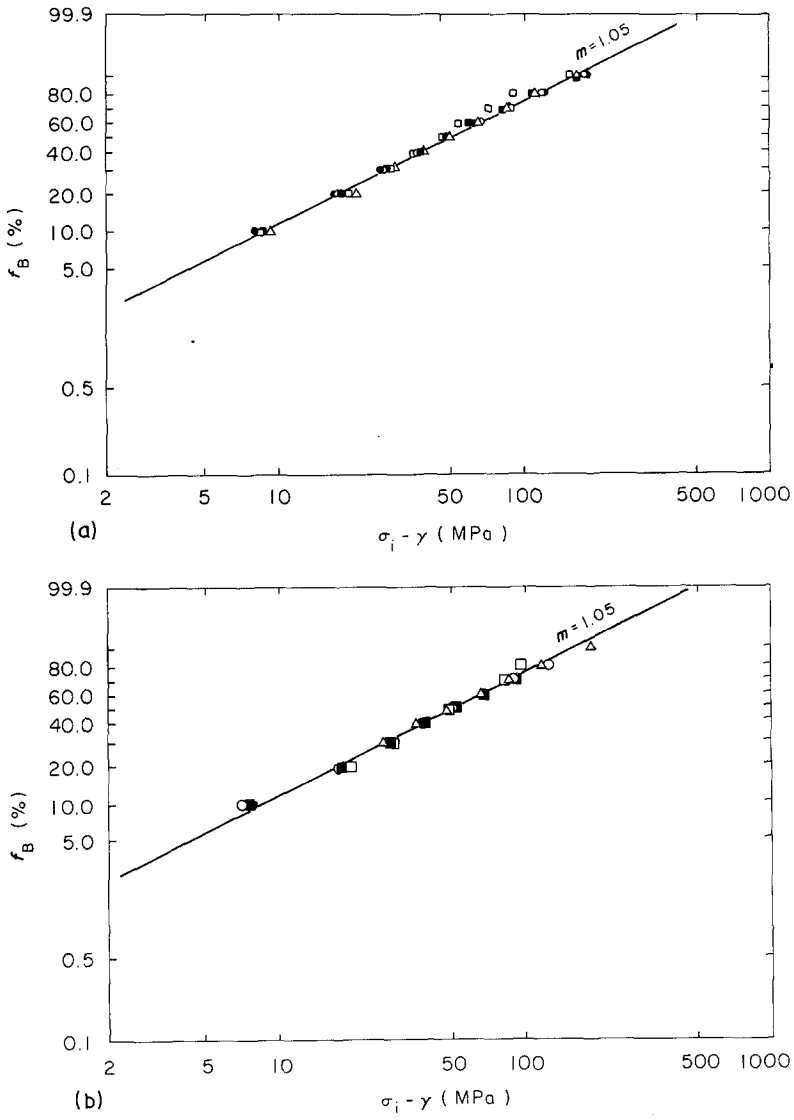

Figure 12 Correlation between volume fraction of the debonded fibre (f_B) and the interfacial stress (σ_i) at Point A in Fig. 11, for B–Al with (a) $V_f = 0.3$: (●) as-fabricated ($\gamma = 73.0$); (□) 1 h ($\gamma = 45.5$); (△) 8 h ($\gamma = 34.5$); (○) 24 h ($\gamma = 72.0$); (■) 72 h ($\gamma = 72.5$). (b) $V_f = 0.5$: (●) as-fabricated ($\gamma = 67.8$); (□) 1 h ($\gamma = 51.5$); (△) 8 h ($\gamma = 49.0$); (○) 24 h ($\gamma = 68.5$); (■) 72 h ($\gamma = 81.5$).

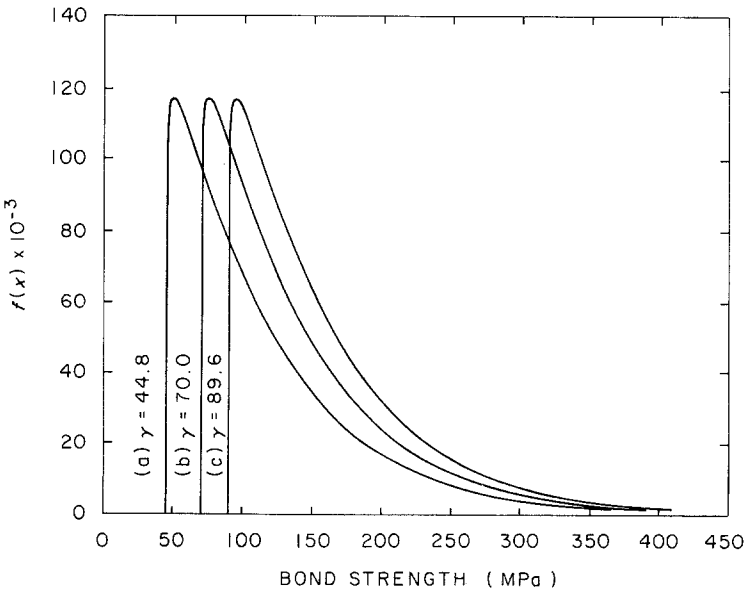

Figure 13 The distribution of the fibre–matrix bond strength estimated by a three-parameter Weibull model for (a) γ = 44.8 MPA, (b) γ = 70 MPa, (c) γ = 89.6 MPa.

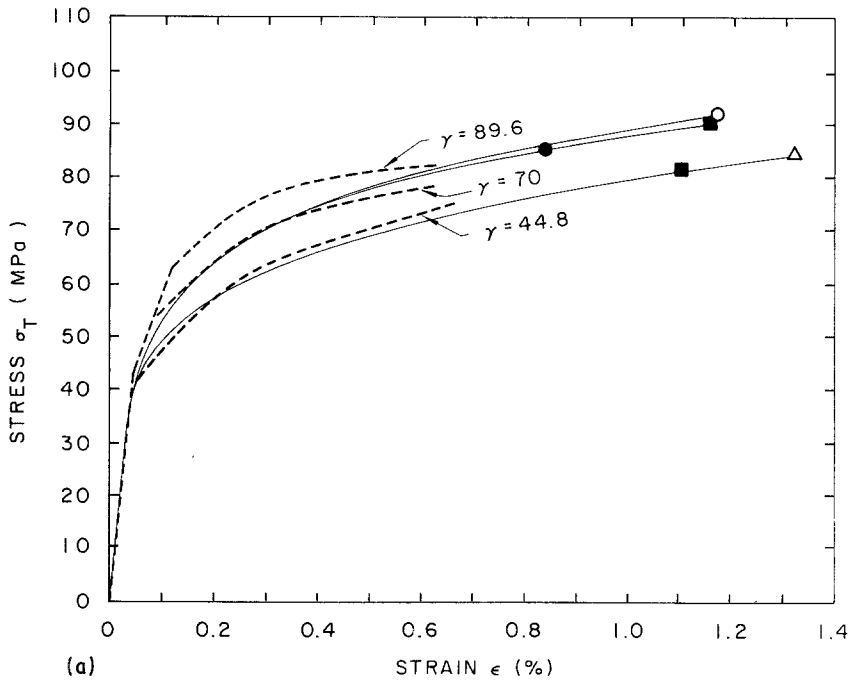

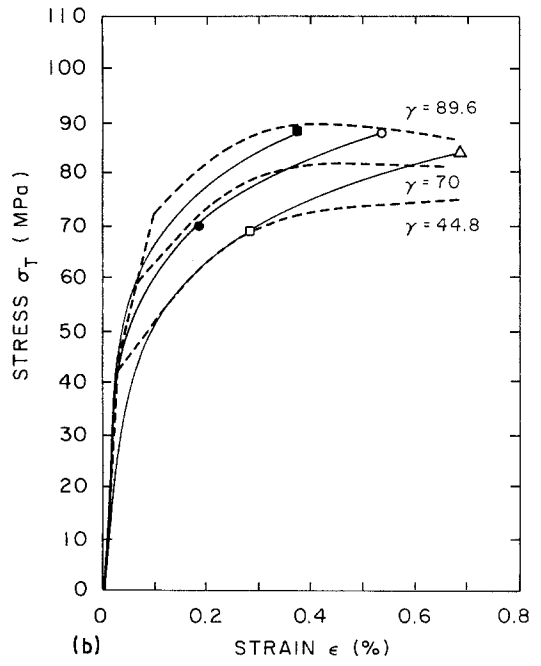

Figure 14 The effect of exposure time on the stress–strain curves for (a) V_f = 0.3 and (b) V_f = 0.5 where solid and dashed curves denote the experimental and analytical results, respectively. (●) As-fabricated, (□) 1 h, (△) 8 h, (○) 24 h, (■) 72 h.

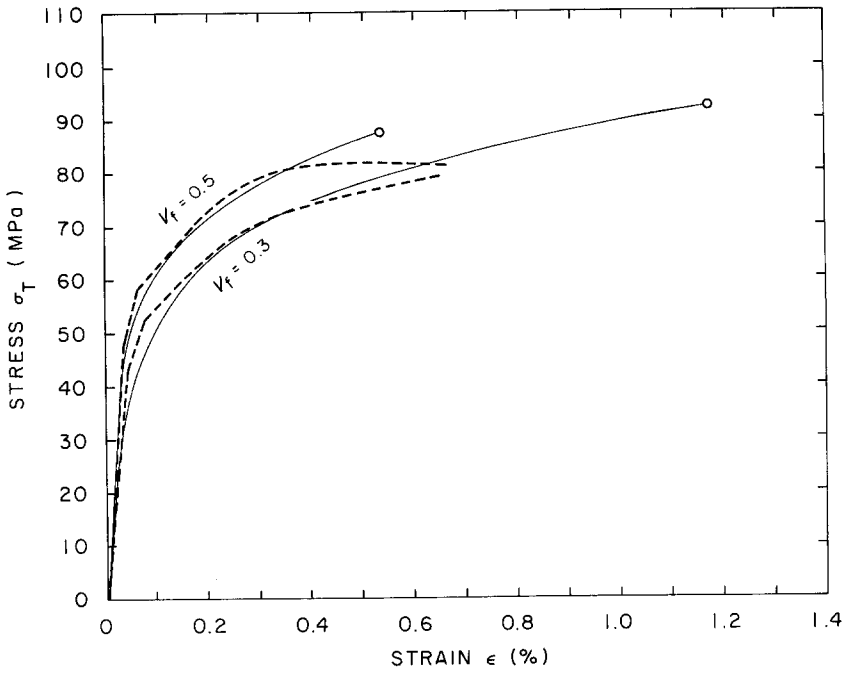

Figure 15 The effect of the fibre volume fraction on the stress–strain behaviour. Comparison between (– – –) theory and (——) experiment; for $t = 24$ h where in the theory $\gamma = 70$ MPa was used.

from interfacial debonding to fibre splitting. According to Adams [5], the fibre splitting occurs at this stress. Hence, if the normal stress along the x_1 axis at point A (Fig. 11) exceeds 260 MPa, the fibre splitting mode is assumed to take place in our analysis.

Based on Eshelby's model and Equation 12 and 13 we have predicted the stress–strain curves for $\gamma = 44.8$, 70.0 and 89.6 MPa, and the results are plotted as dashed curves for $V_f = 0.3$ and 0.5 in Figs 14a and b, respectively, where the experimental results are also shown as solid curves. In Fig. 14 the fracture points of the experimental curves are denoted by various symbols corresponding to the various exposure times (see caption). It follows from Fig. 14 that γ is strongly related to the initial interfacial bond strength. Thus it can be concluded that the longer the exposure time is, the stronger the interfacial bond becomes, except for the case of as-fabricated composite where the interfacial bond is considered strong as described in the previous section. To examine the effect of the volume fraction of fibre, V_f, on the stress–strain curve of the thermally exposed composite, we have applied the present model to the case of $t = 24$ h and $\gamma = 70$ MPa and the results are plotted as dashed curves in Fig. 15, where the corresponding experimental results are also plotted as solid curves. It can be seen from Figs 14 and 15 that reasonably good agreement between the analytical and experimental results is obtained except for the fracture point.

5. Conclusions

The effect of isothermal exposure time at 500° C on the transverse mechanical properties and stress–strain behaviour of 30 and 50 vol % continuous boron fibre reinforced 1100 composites has been investigated experimentally.

Theoretical considerations using Eshelby's theory have then been made to predict the non-linearity of the stress–strain behaviour. This investigation led to the following conclusions:

1. The fibre–matrix interfacial reaction gives rise to an increase of the fibre–matrix bond strength. Consequently, the fracture mode undergoes a transition from interfacial debonding to fibre splitting with increasing exposure time.
2. The initial transverse Young's modulus of a continuous fibre reinforced metal matrix composite is well predicted using Eshelby's theory and is almost independent of the isothermal exposure condition.
3. Stress–strain behaviour depends on the isothermal exposure condition, and the curve tends to rise with increasing fibre–matrix bond strength resulting from the fibre–matrix reaction.
4. The non-linearity of the transverse tensile stress–strain behaviour can be explained qualitatively by the present theoretical model, and reasonable agreement between theory and experiment is obtained.
5. In order to predict the ultimate transverse tensile strength of a continuous fibre reinforced metal matrix composite as well as its fracture strain, further consideration is required.

Acknowledgements

The authors are grateful to Toray Industries, Inc., Japan, for financial support and to the Center for Composite Materials, University of Delaware, for partial support; valuable comments from Dr H. Hatta, Mitsubishi Electric Corp., Japan, and cooperation with the microhardness measurements by the Leco Corporation are also appreciated.

Appendix A

F^i_{11}, F^i_{21}, F^i_{31}, F^i_{13}, F^i_{23} and F^i_{33} in Equations 10 and B2 are defined by

$$F^A_{11} = \frac{1}{P_A}[(B^A_2 C^A_3 - B^A_3 C^A_2) D_1 + (B^A_3 C^A_1 - B^A_1 C^A_3) D_2 + (B^A_1 C^A_2 - B^A_2 C^A_1) D_2]$$

$$F^A_{21} = \frac{1}{P_A}[(A^A_3 C^A_2 - A^A_2 C^A_3) D_1 + (A^A_1 C^A_3$$

$$- A_3^A C_1^A) D_2 + (A_2^A C_1^A - A_1^A C_2^A) D_2]$$

$$F_{31}^A = \frac{1}{P_A}[(A_2^A B_3^A - A_3^A B_2^A) D_1 + (A_3^A B_1^A - A_1^A B_3^A) D_2 + (A_1^A B_2^A - A_2^A B_1^A) D_2] \quad \text{(A1)}$$

$$F_{13}^A = \frac{1}{P_A}[-2(B_2^A C_3^A - B_3^A C_2^A) + (B_3^A C_1^A - B_1^A C_3^A) + (B_1^A C_2^A - B_2^A C_1^A)]\mu_f$$

$$F_{23}^A = \frac{1}{P_A}[-2(A_3^A C_2^A - A_2^A C_3^A) + (A_1^A C_3^A - A_3^A C_1^A) + (A_2^A C_1^A - A_1^A C_2^A)]\mu_f$$

$$F_{33}^A = \frac{1}{P_A}[-2(A_2^A B_3^A - A_3^A B_2^A) + (A_3^A B_1^A - A_1^A B_3^A) + (A_1^A B_2^A - A_2^A B_1^A)]\mu_f$$

$$F_{11}^B = \frac{1}{P_B}[-(B_2^B C_3^B - B_3^B C_2^B) E_m + (B_3^B C_1^B - B_1^B C_3^B) D_2 + (B_1^B C_2^B - B_2^B C_1^B) D_2]$$

$$F_{21}^B = \frac{1}{P_B}[-(A_3^B C_2^B - A_2^B C_3^B) E_m + (A_1^B C_3^B - A_3^B C_1^B) D_2 + (A_2^B C_1^B - A_1^B C_2^B) D_2]$$

$$F_{31}^B = \frac{1}{P_B}[-(A_2^B B_3^B - A_3^B B_2^B) E_m + (A_3^B B_1^B - A_1^B B_3^B) D_2 + (A_1^B B_2^B - A_2^B B_1^B) D_2] \quad \text{(A2)}$$

$$F_{13}^B = \frac{1}{P_B}[(B_3^B C_1^B - B_1^B C_3^B) + (B_1^B C_2^B - B_2^B C_1^B)]\mu_f$$

$$F_{23}^B = \frac{1}{P_B}[(A_1^B C_3^B - A_3^B C_1^B) + (A_2^B C_1^B - A_1^B C_2^B)]\mu_f$$

$$F_{33}^B = \frac{1}{P_B}[(A_3^B B_1^B - A_1^B B_3^B) + (A_1^B B_2^B - A_2^B B_1^B)]\mu_f$$

where

$$P_i = \begin{vmatrix} A_1^i & B_1^i & C_1^i \\ A_2^i & B_2^i & C_2^i \\ A_3^i & B_3^i & C_3^i \end{vmatrix} \quad \text{(A3)}$$

$$A_1^A = (\bar{\lambda} + 2\bar{\mu})(1 - f_A) S_{1111} + \bar{\lambda}(1 - f_A)(S_{2211} + S_{3311}) + (\bar{\lambda} f_A + \lambda) + 2(\bar{\mu} f_A + \mu)$$

$$B_1^A = (\bar{\lambda} + 2\bar{\mu})(1 - f_A) S_{1122} + \bar{\lambda}(1 - f_A)(S_{2222} + S_{3322}) + (\bar{\lambda} f_A + \lambda)$$

$$C_1^A = (\bar{\lambda} + 2\bar{\mu})(1 - f_A) S_{1133} + \bar{\lambda}(1 - f_A)(S_{2233} + S_{3333}) + (\bar{\lambda} f_A + \lambda)$$

$$A_1^B = (1 - f_B)[(\lambda_m + 2\mu_m)(S_{1111} - 1) + \lambda_m(S_{2211} + S_{3311})] \quad \text{(A4)}$$

$$B_1^B = (1 - f_B)[(\lambda_m + 2\mu_m) S_{1122} + \lambda_m(S_{2222} + S_{3322} - 1)]$$

$$C_1^B = (1 - f_B)[(\lambda_m + 2\mu_m) S_{1133} + \lambda_m(S_{2233} + S_{3333} - 1)]$$

$$A_2^i = \bar{\lambda}(1 - f_i)(S_{1111} + S_{3311}) + (\bar{\lambda} + 2\bar{\mu})(1 - f_i) S_{2211} + (\bar{\lambda} f_i + \lambda)$$

$$B_2^i = \bar{\lambda}(1 - f_i)(S_{1122} + S_{3322}) + (\bar{\lambda} + 2\bar{\mu})(1 - f_i) S_{2222} + (\bar{\lambda} f_i + \lambda) + 2(\bar{\mu} f_i + \mu)$$

$$C_2^i = \bar{\lambda}(1 - f_i)(S_{1133} + S_{3333}) + (\bar{\lambda} + 2\bar{\mu})(1 - f_i) S_{2233} + (\bar{\lambda} f_i + \lambda) \quad \text{(A6)}$$

$$A_3^i = \bar{\lambda}(1 - f_i)(S_{1111} + S_{2211}) + (\bar{\lambda} + 2\bar{\mu})(1 - f_i) S_{3311} + (\bar{\lambda} f_i + \lambda)$$

$$B_3^i = \bar{\lambda}(1 - f_i)(S_{1122} + S_{2222}) + (\bar{\lambda} + 2\bar{\mu})(1 - f_i) S_{3322} + (\bar{\lambda} f_i + \lambda)$$

$$C_3^i = \bar{\lambda}(1 - f_i)(S_{1133} + S_{2233}) + (\bar{\lambda} + 2\bar{\mu})(1 - f_i) S_{3333} + (\bar{\lambda} f_i + \lambda) + 2(\bar{\mu} f_i + \mu)$$

In Equations A3 and A6, superscript and subscript i denote A (for Ω_A) or B (for Ω_B).

$$\bar{\lambda} = \lambda_f - \lambda_m$$
$$\bar{\mu} = \mu_f - \mu_m \quad \text{(A7)}$$

$$D_1 = -[\bar{\lambda}(1 - 2\nu_m) + 2\bar{\mu}]$$
$$D_2 = 2\bar{\mu}\nu_m - \bar{\lambda}(1 - 2\nu_m) \quad \text{(A8)}$$

where λ_j and μ_j are Lame's constants of the i phase (j = m and f), and E_m and ν_m are Young's modulus and Poisson's ratio of the matrix, respectively; S_{ijkl} is Eshelby's tensor [21].

Appendix B

K_1 and K_2 in Equation 11 are given by

$$K_1 = \frac{1 - (f_A + f_B)}{1 - (f_A + f_B) - (L_1^A + L_1^B)}$$
$$K_2 = \frac{L_3^B - L_3^A}{1 - (f_A + f_B) - (L_1^A + L_1^B)} \quad \text{(B1)}$$

where with Equations A1 and A2, L_1^i and L_3^i (i = m and f) are given as

$$L_1^i = f_i(1 - f_i)(G_1 F_{11}^i + G_2 F_{21}^i + G_3 F_{31}^i)$$
$$L_3^i = f_i(1 - f_i)(G_1 F_{13}^i + G_2 F_{23}^i + G_3 F_{33}^i) \quad \text{(B2)}$$

where G_1, G_2 and G_3 are defined by Equation A9 as

$$G_1 = H_{11} - \frac{H_{21} + H_{31}}{2}$$
$$G_2 = H_{12} - \frac{H_{22} + H_{32}}{2} \quad \text{(B3)}$$
$$G_3 = H_{13} - \frac{H_{23} + H_{33}}{2}$$

H_{ij} are defined by

$$H_{11} = \frac{1}{1 + \nu_m}\left(\frac{\nu_m}{1 - 2\nu_m}(S_{1111} + S_{2211} + S_{3311} - 1) + S_{1111} - 1\right)$$

$$
\begin{aligned}
H_{12} &= \frac{1}{1+\nu_m}\left(\frac{\nu_m}{1-2\nu_m}(S_{1122}+S_{2222}\right. \\
&\quad \left. +S_{3322}-1)+S_{1122}\right) \\
H_{13} &= \frac{1}{1+\nu_m}\left(\frac{\nu_m}{1-2\nu_m}(S_{1133}+S_{2233}\right. \\
&\quad \left. +S_{3333}-1)+S_{1133}\right) \\
H_{21} &= \frac{1}{1+\nu_m}\left(\frac{\nu_m}{1-2\nu_m}(S_{1111}+S_{2211}\right. \\
&\quad \left. +S_{3311}-1)+S_{2211}\right) \\
H_{22} &= \frac{1}{1+\nu_m}\left(\frac{\nu_m}{1-2\nu_m}(S_{1122}+S_{2222}\right. \\
&\quad \left. +S_{3322}-1)+S_{2222}-1\right) \\
H_{23} &= \frac{1}{1+\nu_m}\left(\frac{\nu_m}{1-2\nu_m}(S_{1133}+S_{2233}\right. \\
&\quad \left. +S_{3333}-1)+S_{2233}\right) \\
H_{31} &= \frac{1}{1+\nu_m}\left(\frac{\nu_m}{1-2\nu_m}(S_{1111}+S_{2211}\right. \\
&\quad \left. +S_{3311}-1)+S_{3311}\right) \\
H_{32} &= \frac{1}{1+\nu_m}\left(\frac{\nu_m}{1-2\nu_m}(S_{1122}+S_{2222}\right. \\
&\quad \left. +S_{3322}-1)+S_{3322}\right) \\
H_{33} &= \frac{1}{1+\nu_m}\left(\frac{\nu_m}{1-2\nu_m}(S_{1133}+S_{2233}\right. \\
&\quad \left. +S_{3333}-1)+S_{3333}-1\right)
\end{aligned}
\tag{B4}
$$

References

1. A. G. METCALFE (ed), "Interfaces in Metal Matrix Composites", Vol. 1 (Academic Press, New York, 1974).
2. T. KYONO, I. W. HALL and M. TAYA, *J. Mater. Sci.* in press.
3. G. JACOBSEN, in "Progress in Science and Engineering of Composites", edited by T. Hayashi *et al.*, ICCM-IV Tokyo, 1982, p. 1323.
4. D. F. ADAMS and D. R. DONER, *J. Compos. Mater.* 7 (1967) 152.
5. D. F. ADAMS, *ibid.* **4** (1970) 310.
6. J. M. LIN, P. E. CHEN and A. T. DIBENEDETTO, *Polym. Eng. Sci.* **11** (4) (1971) 344.
7. M. F. AMATEAU and D. L. DULL, in "Failure Modes in Composites IV", edited by J. A. Cornie and F. W. Crossman (TMS-AIME, New York, 1977) p. 336.
8. K. M. PREWO and K. G. KREIDER, *Met. Trans.* **3** (1972) 2201.
9. G. A. COOPER and A. KELLY, ASTM STP 452 (American Society for Testing and Materials, Philadelphia, 1969) p. 90.
10. D. RIGGS, in "New Developments and Applications in Composites", edited by D. Kuhlman-Wilsdorf and W. C. Harrigan (TMS-AIME, New York, 1979) p. 252.
11. J. D. ESHELBY, *Proc. R. Soc.* **A241** (1957) 376.
12. K. G. KREIDER, in "Metallic Matrix Composites", Vol. 4, (Academic Press, New York, 1974) p. 429.
13. H. H. GRIMES, R. A. LAD and J. E. MAISEL, *Met. Trans. A.* **8A** (1977) 1999.
14. Y. MIKATA and M. TAYA, *J. Compos. Mater.* **19** (1985) 554.
15. W. H. KIM, M. J. KOCZAK and A. LAWLEY, in Proceedings of ICCM/2, edited by B. Norton *et al.* (TMS-AIME, New York, 1978) p. 487.
16. A. SKINNER, M. J. KOCZAK and A. LAWLEY, *Met. Trans. A.* **13A** (1982) 289.
17. K. TANAKA and T. MORI, *Acta Metall.* **18** (1970) 931.
18. A. DAIMARU and M. TAYA, in "Progress in Science and Engineering of Composites", edited by T. Hayashi *et al.*, ICCM-IV Tokyo, 1982, 1099.
19. K. TANAKA, T. MORI and T. NAKAMURA, *Phil. Mag.* **21** (1970) 267.
20. M. TAYA and T. W. CHOU, *Int. J. Solid. Struct.* **17** (1981) 553.
21. T. MURA, "Micromechanics of Defects in Solids", (Martinus Nijhoff, The Hague, 1982).
22. M. TAYA and W. G. PATTERSON, *J. Mater. Sci.* **17** (1982) 115.
23. K. TANAKA, K. NARITA and T. MORI, *Acta Metall.* **20** (1972) 297.

Received 16 January
and accepted 14 March 1986